Functional characterization of macaque insula using task-based and resting-state fMRI

Lotte Sypré, Jean-Baptiste Durand, Koen Nelissen

NeuroImage 276 (2023) 120217

Contents lists available at ScienceDirect

NeuroImage

journal homepage: www.elsevier.com/locate/neuroimage

Functional characterization of macaque insula using task-based and resting-state fMRI

Lotte Sypré[a,b], Jean-Baptiste Durand[c], Koen Nelissen[a,b,*]

[a] Laboratory for Neuro- & Psychophysiology, Department of Neurosciences, KU Leuven, 3000 Leuven, Belgium
[b] Leuven Brain Institute, KU Leuven, 3000 Leuven, Belgium
[c] CNRS CERCO UMR 5549, Toulouse, France

ARTICLE INFO

Keywords:
Insula
fMRI
rhesus monkey
visual
motor
vestibular
gustatory

ABSTRACT

Neurophysiological investigations over the past decades have demonstrated the involvement of the primate insula in a wide array of sensory, cognitive, affective and regulatory functions, yet the complex functional organization of the insula remains unclear. Here we examined to what extent non-invasive task-based and resting-state fMRI provides support for functional specialization and integration of sensory and motor information in the macaque insula. Task-based fMRI experiments suggested a functional specialization related to processing of ingestive/taste/distaste information in anterior insula, grasping-related sensorimotor responses in middle insula and vestibular information in posterior insula. Visual stimuli depicting social information involving conspecific's lip-smacking gestures yielded responses in middle and anterior portions of dorsal and ventral insula, overlapping partially with the sensorimotor and ingestive/taste/distaste fields. Functional specialization/integration of the insula was further corroborated by seed-based whole brain resting-state analyses, showing distinct functional connectivity gradients across the anterio-posterior extent of both dorsal and ventral insula. Posterior insula showed functional correlations in particular with vestibular/optic flow network regions, mid-dorsal insula with vestibular/optic flow as well as parieto-frontal regions of the sensorimotor grasping network, mid-ventral insula with social/affiliative network regions in temporal, cingulate and prefrontal cortices and anterior insula with taste and mouth motor networks including premotor and frontal opercular regions.

1. Introduction

The primate insular cortex has been the subject of numerous investigations in the past decades, showing a complex anatomical and connectional organization, and suggesting a crucial role in a wide array of sensory, cognitive, affective and regulatory functions (Evrard, 2019). Intracortical microstimulation studies in awake monkeys demonstrated that the insula contains three main motor subfields: a sensorimotor field occupying the mid-posterior dorsal portion of the insula and related to motor responses involving mainly the hand but also the mouth, face, upper and lower limbs, a mid-posterior ventral field related to affiliative and social interaction behavior, and an anterior field related to ingestive and disgust behavior (Caruana et al., 2011; Jezzini et al., 2012).

In addition to these motor behaviors elicited using electrical microstimulation, invasive neurophysiological studies provided evidence for functional specializations of macaque insular subregions, suggesting taste related responses in anterior portions of the insula (Yaxley et al., 1990; Ogawa, 1994), sensorimotor responses in mid-dorsal insula (Schneider et al., 1993; Ishida et al., 2015; Baumgärtner et al., 2006, 2010), processing of vestibular information in posterior insula (Chen et al., 2010, 2021), and representation of social information related to conspecifics in ventral insula (Remedios et al., 2009). Although former invasive recordings provided detailed information with respect to single unit response properties in the insula, these studies rarely examined the entire insula, leaving it unclear to what extent different sensations or motor actions modulate specific insular subregions.

In the past decades, functional MRI in non-human primates has proven an invaluable tool for understanding the functional organization of the primate brain (Vanduffel et al., 2014). Comparative fMRI studies allow establishing homologies and/or differences in the functional organization of brain regions in human and non-human primates (Peeters et al., 2009; Pinsk et al., 2009; Mantini et al., 2012; Joly et al., 2012; Patel et al., 2015) and are essential for integrating human non-invasive neuroimaging data with more detailed invasive anatomical and/or functional data obtained in monkeys. In this study, we employed both task-based and resting-state fMRI to examine the functional orga-

* Corresponding author: Koen Nelissen, Lab for Neuro- & Psychophysiology, Department of Neurosciences, KU Leuven, O&N2 Campus Gasthuisberg, Herestraat 49, bus 1021, 3000 Leuven, Belgium.
E-mail address: koen.nelissen@kuleuven.be (K. Nelissen).

https://doi.org/10.1016/j.neuroimage.2023.120217.
Received 31 January 2023; Received in revised form 13 May 2023; Accepted 1 June 2023
Available online 2 June 2023.

nization of the macaque monkey insula. For our task-based fMRI investigations, we examined processing of information across several different modalities: gustatory (taste and distaste/disgust perception), sensorimotor (grasping execution), visual (observation of conspecific lip-smacking face expressions) and vestibular (galvanic vestibular stimulation). Functional specialization/integration within the insula was further addressed using seed-to-whole-brain and seed-to-ROI resting-state analyses. More specifically, we examined to what extent resting-state fMRI data provided support for distinct versus overlapping functional connectivity of macaque insular subregions with key regions of the vestibular/optic flow, sensorimotor (or somatomotor) grasping, gustatory/ingestive and social/affiliative brain networks.

2. Materials and Methods

2.1. Subjects

In total, ten macaque monkeys (M1 – M10, *Macaca mulatta*, 6 males, 4 females, 5–9 kg) participated in the resting-state and task-based fMRI experiments. Eight macaque monkeys participated in the awake resting-state fMRI experiments (M1 – M8, *Macaca mulatta*, 6 males, 2 females, 5–8 kg). Two of these monkeys (M1 and M2, both males) also participated in the majority of the task-based fMRI experiments (taste and distaste/disgust processing, grasping execution, observation of facial expressions). Two additional monkeys (M9 and M10, *Macaca mulatta*, both females, 5–8 kg) participated in the galvanic vestibular stimulation experiment. All animal care and experimental procedures followed the national and European guidelines and were approved by either the animal ethical committee of KU Leuven (experiments involving monkeys M1 – M8) or the French Ministry of Research (MP/03/34/10/09) and the local ethics committee of Toulouse University (CNREEA code: C2EA–14) (experiments involving monkeys M9 and M10).

2.2. FMRI habituation protocol

Prior to scanning the subjects for the different awake task-based or resting-state fMRI experiments, monkeys were habituated to the scanner environment. Following previously described methods, monkeys were adapted to physical restraint in a small plastic box (seated in the so-called “sphinx” position) and habituated to the sounds of MR scanning using a mock MR bore in the training setup (Vanduffel et al., 2001). Prior to the actual fMRI scans, most monkeys also underwent several training sessions in the MR scanner. This overall procedure ensured that during the actual scanning sessions, monkeys performed their tasks without obvious behavioral signs of distress.

2.3. Task-based fMRI experiments

2.3.1. Taste localizer

For the taste localizer fMRI experiment, monkeys sat in a sphinx position in a custom-made plastic monkey chair while they were required to maintain fixation within a $2 \times 2^{\circ}$ window centered around a red fixation point ($0.35 \times 0.35^{\circ}$) positioned in the center of the screen placed in front of them. Eye position was monitored through pupil position and corneal reflection (Iscan). While fixating, monkeys received random blocks of different liquid tastants (sweet (0.3 M sucrose), sour (0.01 M citric acid) or distilled water). Sweet and sour solutions were prepared using distilled water. For this taste localizer experiment, a block design was used with alternating blocks of sweet or sour solution or distilled water. A typical run consisted of five start volumes, followed by blocks (20 s) of either sweet liquid, sour liquid or distilled water. Every 20 s block was followed by a 10 s period during which distilled water was delivered in order to rinse out residual taste. This sequence was repeated three times per run, resulting in 185 volumes (6 min 10 s). Condition orders were randomized across runs. Runs with a fixation performance above 90% were included in a fixed-effects group data analysis, resulting in 58 runs collected across two different scan sessions (29 runs from each monkey).

2.3.2. Distaste/disgust localizer

For the distaste/disgust fMRI localizer, monkeys were required to maintain fixation within a $2 \times 2^{\circ}$ window centered around a red fixation point ($0.35 \times 0.35^{\circ}$) positioned in the center of the screen. Eye position was monitored through pupil position and corneal reflection (Iscan). While fixating, the monkeys received random blocks of different liquid tastants. These liquid tastants included two different concentrations of sour solution (0.01 M or 1 M citric acid dissolved in distilled water) or distilled water only. Using video analysis of facial expressions, we confirmed that the lowest concentration of sour liquid (0.01 M citric acid) did not yield behavioural facial motor responses typical for distaste/disgust facial expressions (Parr et al., 2010), while administering the highest concentration of sour liquid (1 M citric acid) yielded prototypical distaste/disgust expressions, including nose wrinkle, open mouth and tongue protrusion (Parr et al., 2010). A typical distaste/disgust localizer run started with 15 start volumes, followed by alternating blocks of a high sour, low sour and distilled water (each lasting for 10 s), each followed by a 20 s block of distilled water. The order of conditions was repeated four times per run and randomized across runs, which yielded runs of 240 volumes (8 min). FMRI fixed-effects group analysis consisted of 26 runs (13 runs from each monkey) across three different scan sessions in which runs with an overall fixation performance above 90% were selected.

2.3.3. Grasping execution localizer

The grasping execution motor task has been previously described in Sharma et al. (2018). Motor runs consisted of blocks of 3 conditions: reach-and-grasp execution, reach-only execution and fixation only. For the reach-and-grasp task, monkeys were trained to grasp three spheres of different sizes (16, 23 or 40 mm radius) with their right hand. Motor tasks were performed in the dark. An MR-compatible pneumatic motor was used to rotate a disk holding the three objects (Nelissen and Vanduffel, 2011; Nelissen et al, 2018; Sharma et al., 2018). To initiate a grasping trial, the monkey had to place his right hand in the start position and fixate on a green fixation point displayed in the center of the screen. After a random period (500 – 1500 ms), the green fixation point switched to blue, cueing the monkey to reach and grasp the sphere in front of him with his right hand. Subsequently, the monkey had to lift the object 5 mm upwards and hold it for at least 500 ms to receive a juice reward. As soon as the monkey returned his hand to the start position while maintaining fixation, a new trial was initiated by presenting the green cue again. Optic fibers placed at the start position and near the object positions as well as three other locations along the reaching trajectory enabled tracking of the hand and arm location and timing of motor execution. Monkeys also performed a reach-only motor task as a control. During these reach-only trials, the monkey had to reach forward and place its hand onto an empty slot of the rotating disk for at least 500 ms to receive a liquid reward. For reach-only trials, all visual cues and timing parameters remained exactly the same as for the reach-and-grasp trials. During the fixation baseline condition, the monkeys needed to maintain fixation within a $2 \times 2^{\circ}$ window centered around a red fixation point ($0.35 \times 0.35^{\circ}$) positioned in the center of the screen while keeping their right hand in the start position in order to receive a juice reward (Sharma et al., 2018; Nelissen et al., 2018; Nelissen and Vanduffel, 2011). Eye movements were recorded during the experiments (Iscan). Functional MRI runs of the grasping localizer experiment consisted of alternating blocks of reach-and-grasp, reach-only and fixation-only trials (Sharma et al., 2018). A typical run consisted of five start volumes followed by a sequence of blocks of grasp 16 mm sphere – fix only – grasp 40 mm sphere – fix only – grasp 23 mm sphere – fix only – reach-only – fix only – fixation only (baseline) – fix only. Each of these blocks lasted for 30 s and this sequence was repeated

once per run, which resulted in 305 volumes (10 min 10 s) per run. For monkey M2, the same block design was used, but with a different order of object presentation (23 mm, 16 mm and 40 mm sphere respectively) compared to monkey M1. For the grasping localizer data, we reanalysed a subset of the data (6 runs for monkey M1 and 6 runs for monkey M2) previously published in Sharma et al. (2018).

2.3.4. Visual facial expression localizer

During the face expression localizer, monkeys received juice rewards for keeping fixation within a 2 × 2° window centered on a red dot (0.35 × 0.35°) in the center of the screen while different visual stimuli were presented. Eye position was monitored through pupil position and corneal reflection (Iscan). Visual stimuli included frontal view video clips of conspecific emotional lip-smacking face gestures. In total, four subjects (3 males and 1 female) were recorded while performing this affiliative lip-smacking behaviour. All four original videos were flipped along the vertical axis to create a second set of lip-smack videos, increasing stimulus batch size to eight videos. Scrambled control stimuli were generated from each lip-smack video by phase scrambling each frame of the video sequences using Matlab (Nelissen et al., 2005, 2006). In total, eight different lip-smack videos and their corresponding scrambled controls were used in the experiment. All videos measured 11.8 × 11.8 visual degrees and had a duration of 2 s. For the lip-smack facial expression experiment, a block design was used consisting of alternating 30 s blocks of lip-smack face gestures, scrambled controls and fixation-only baseline. During a typical lip-smack or scrambled control block, 15 videos were presented randomly out of the batch of eight different videos. Each sequence of conditions was presented thrice in one run and randomized across runs. Thus, each run included 185 volumes (6 min 10 s). For this experiment, fixed-effects group analysis consisted of 64 runs in total (32 runs from each monkey) collected across one (for M1) or two (for M2) different scan sessions.

2.3.5. Galvanic vestibular localizer

For the galvanic vestibular stimulation, two gold electrodes (diameter 1 cm) were placed on the mastoid behind the ears of the monkeys. Stimulation consisted of a sinusoidal current (to avoid sharp on/off transients) with a frequency of 1 Hz and an amplitude of ± 2.5 mA. A computer in the MRI control room sent a voltage to a USB data acquisition card (NI USB-6009, DAQ 8AD 2DA 14 bit 48kS/s Labview), allowing to regulate the frequency and amplitude of the voltage. The NI card sent the voltage to a current-limited stimulator (Digitimer, UK; model DS5) which converted this voltage into current and, after passing through the MR filter, delivered the resulting current into the electrodes placed behind the ears of the monkey. During the galvanic vestibular stimulation experiments, monkeys were anesthetized using a mixture of medetomidine (0.04 mg/kg) and ketamine (10 mg/kg). For the galvanic vestibular stimulation experiment, a block design consisting of blocks of bilateral stimulation and no stimulation was used. Each block lasted for 12 volumes or 18 s and was repeated 6 times per run which resulted in runs of 145 volumes (3 min 38 s). In total we used 12 runs per monkey for the analysis, collected in one session for both monkeys M9 and M10.

2.4. Awake resting-state fMRI

During the resting-state scans, monkeys were engaged in a fixation task and had to fixate within a 2 × 2° window centered on a red dot (0.35 × 0.35°) in the center of a screen. The animals received juice rewards for maintaining fixation while eye position was monitored through pupil position and corneal reflection (Iscan). Similar fixation tasks during resting-state fMRI were previously used both in monkey (Mantini et al., 2011; Touroutoglou et al., 2016; Sharma et al., 2019, 2021) and human resting-state studies (Agcaoglu et al., 2019; Patriat et al., 2013; Spadone et al., 2015). While the term 'resting-state' originally reflected measuring correlations of signals between brain regions in the absence of any stimulus or explicit task, fixation tasks have been introduced to avoid alterations between wakefulness and sleep which has shown to affect resting-state results (Tagliazucchi and Laufs, 2014). In non-human primates, this procedure of acquiring resting-state fMRI data using a simple fixation task with rewards (Mantini et al., 2011; Touroutoglou et al., 2016; Sharma et al., 2019) in addition allows for scanning awake monkeys while minimizing body movements and motion artefacts. We refer to our resting-state procedure involving a fixation task as 'resting-state' fMRI. The term 'task-based' fMRI on the other hand was used to describe fMRI sessions involving either explicit changes in task demands (grasp localizer) or sensory stimulation (vestibular, taste, distaste/disgust and visual facial expression localizers).

One resting-state fMRI run lasted for 300 volumes or 10 minutes. For the resting-state fMRI analysis, runs with a fixation percentage below 85% were excluded. In addition, the average correlation across voxel time-series was calculated per run. Runs with values below or above two times the median across runs were considered as outliers and excluded from data analysis (Mantini et al., 2011; Sharma et al., 2019). This resulted in 18 runs from monkey M1, 19 runs from monkey M2, 17 runs from monkey M3, 19 runs from monkey M4, 18 runs from monkey M5, 14 runs from monkey M6, 15 runs from monkey M7, and 19 runs from monkey M8. The resting-state data used in this study are the same as also used in previously published studies (Sharma et al., 2019; Sharma et al., 2021).

2.5. fMRI data acquisition

Task-based fMRI data of experiments described in Sections 2.3.1 – 2.3.4 and resting-state fMRI data (Section 2.4) were acquired with a 3.0 Tesla full-body scanner (Siemens) using a gradient-echo T2*-weighted echo-planar imaging sequence of 40 horizontal slices (time repetition (TR) = 2 s, time echo (TE) = 17 ms, flip angle = 90°, 1.25 × 1.25 × 1.25 mm isotropic voxels). During these experiments, functional images were acquired using a custom-built eight-channel phased-array receive coil and a saddle-shaped, radial transmit-only surface coil (Kolster et al., 2009). Prior to every scanning session, an iron contrast agent (Molday ION, BioPAL in monkey M1 – M4 and MION or Sinerem, Laboratoir Guerbet in monkey M5 – M8) was injected into the femoral or saphenous vein (6 – 12 mg/kg) to enhance spatial selectivity of MR signal changes, thus improving signal-to-noise ratio (Vanduffel et al., 2001; Zhao et al., 2006). For the galvanic vestibular stimulation experiment (monkeys M9 and M10, Section 2.3.5), a 3.0 Tesla clinical MR scanner (Philips Achieva) was used, in addition to a custom eight-channel phased-array coil (RapidBiomed). Blood oxygen level dependent (BOLD) T2*-weighted functional volumes were acquired by gradient echo-planar imaging (GE-EPI: TR = 1500 ms; TE = 30 ms; flip angle = 75°; SENSE factor = 1.6; voxel size = 1.25 × 1.25 × 1.5 mm; 46 axial slices with no inter-slice gap; FOV = 80 × 80 mm).

Resting-state and task-based fMRI data in the two animals (monkey M1 and M2) that were included in most experiments (resting-state and all task-based experiments except galvanic stimulation) and received iron contrast agents prior to scanning, were acquired in a total of nine different sessions over a period of approximately 6 years. Suppl. Table 1 shows a list of the number of scan sessions (related to this study) for both animals in chronological order. To reduce the risk of iron accumulation, 1 g/day deferoxamine mesylate (Desferal®, Novartis; intramuscular injection) was administered after the contrast-enhanced scan sessions, and blood samples were taken regularly to ensure serum iron and ferritin level returned approximately to normal ranges.

2.6. fMRI data preprocessing

Data were corrected for motion-related artefacts by spatially realigning each volume to the first volume of the first run. This so-called re-

alignment produced six vectors (three translations and three rotations along the x-, y- and z-axis) and was performed using statistical parametric mapping (SPM12; RRID:SCR_007037). Subsequently, the motion-corrected functional images were processed with rigid and non-rigid co-registration using JIP software (http://www.nitrc.org/projects/jip/; RRID:SCR_009588) to account for individual monkey anatomy variability. All functional images were co-registered to a template anatomical image (monkey M12; Ekstrom et al., 2008; Nelissen and Vanduffel, 2011). Co-registered functional images were resliced to 1 mm^3 isotropic voxel size and smoothed with a 2.5 mm or 1.5 mm (FWHM) Gaussian kernel using SPM12 for the resting-state fMRI data or task fMRI data respectively (see Sections 2.3 – 2.4), respectively. For the galvanic vestibular stimulation experiment, additional slice-timing correction was used prior to realignment using SPM12.

2.7. Seed-to-brain functional connectivity analyses

In order to examine in a detailed manner the insular functional connectivity to the rest of the brain, we selected in each hemisphere a total of 22 seeds (spheres of 1 mm radius; spaced 2 mm apart; 11 dorsal seeds and 11 ventral seeds in each hemisphere) covering the full anterior-to-posterior extent of the dorsal and the ventral insula (Suppl. Fig. 1). After data preprocessing, band-pass filtering between 0.0025 and 0.05 Hz as well as regression of white matter, ventricle signals and three-dimensional motion parameters was applied. Next, the mean representative time course was calculated by averaging the signal across all voxels within each predefined seed (Mantini et al., 2011; Sharma et al., 2019; Vincent et al., 2007). By calculating the Pearson correlations between the signal of the seed and each voxel of the brain, whole-brain connectivity maps were created. The Fisher's r-to-z transformation was applied to convert individual whole-brain connectivity maps to z-scores after which a fixed-effect analysis created group-level correlation maps (Mantini et al., 2011; Touroutoglou et al., 2016; Sharma et al., 2019). The latter were finally thresholded at $z > 2.0$ (Touroutoglou et al., 2016). Finally, the group-level correlation maps of every single seed were displayed on a flattened representation of monkey M12's anatomical template using Caret software (version v5.65). In order to control the false discovery rate in the seed-to-brain analyses, we used the two-stage step-up procedure by Benjamini et al., 2006 (https://www.mathworks.com/matlabcentral/fileexchange/27423-two-stage-benjamini-krieger-yekutieli-fdr-procedure). Suppl. Figs 3 and 4 show which voxels survive FDR correction and at which significance level (color code: dark blue: p<0.01 & FDR>0.05; light blue: FDR<0.05 & FDR>0.01; orange: FDR<0.01 & FDR>0.001; yellow: FDR<0.001).

2.8. Seed-to-ROI functional connectivity network analyses

In order to quantify functional connectivity between insular seeds and the vestibular/optic flow, sensorimotor grasping, gustatory/ingestive and social/affiliative networks, we defined ROIs in key areas belonging to these functional networks, based upon either D99 atlas or anatomical landmarks based upon previous anatomical and/or functional studies. For the *vestibular/optic flow network*, we defined a ROI for several regions previously shown to play a role in processing vestibular and/or optic flow information: area VIP in the intraparietal sulcus, area MSTd in the upper bank of the STS, area 23 in the posterior cingulate cortex (including optic flow/vestibular region pmCSv) and area VPS near the posterior end of the Sylvian fissure (Cottereau et al. 2017; Chen et al., 2011, 2016; De Castro et al., 2021). For the *sensorimotor grasping network*, ROIs were defined in intraparietal area AIP, ventral premotor area F5a, hand representation of S1 and parietal area PE (Belmalih et al., 2009; Gerbella et al., 2011; Nelissen and Vanduffel, 2011; Borra et al., 2017; Sharma et al., 2018, 2019). In the *gustatory/ingestive network*, we defined a ROI in the mouth representation of area F4 (F4 ventral) (Kurata, 2018; Maranesi et al., 2012) and in frontal operculum regions PrCO, DO and GrFO involved in gustatory processing and orofacial movements (Gerbella et al., 2016; Sharma et al., 2019; Ferrari et al., 2017). Finally, four ROIs were defined in the *social/affiliative* network. These ROIs encompassed regions processing social cues and emotional aspects of sensory stimuli (orbitofrontal area 12m), a region involved in the observation and production of emotional facial expressions (anterior cingulate area 24; Livneh et al., 2012), and finally two higher-order visual areas in temporal cortex (IPa and area TEm), playing a role in processing social cues involving others (Perrett et al., 1989; Tsao and Livingstone, 2008; Cui et al., 2023). For visualizing functional correlations of insular seeds with the 16 functional ROIs belonging to the vestibular/optic flow, sensorimotor grasping, gustatory/ingestive and social/affiliative networks, positive z-scores for each of the dorsal and ventral insular seeds were plotted in spider charts. Since we were mostly interested in seeds showing positive correlations, negative z-scores were set to 0 for display purposes in the spider charts.

2.9. General linear model fitting and univariate whole-brain analysis for task localizers

For the task-based fMRI data, a general linear model (GLM) was used to estimate the response amplitude at each voxel (SPM12) following previously described procedures (Friston et al., 1994; Vanduffel et al., 2001). A MION hemodynamic response function was convolved with a boxcar model to represent the stimulus conditions for the fMRI experiments that were done using iron contrast agent (Vanduffel et al., 2001). To account for artefacts due to head and eye-movements, we included nine regressors of no interest in the GLM model. These regressors corresponded to three rotations and three translations along x-, y- and z-axis (head motion) as well as the horizontal and vertical component of the eye movement and pupil diameter. For each run, this GLM fitting resulted in a map of beta estimates (regression weights) for each condition of interest and for the nine regressors of no interest. GLM analyses were performed for each subject separately. Since the galvanic vestibular stimulation data were acquired using BOLD measurements, the corresponding BOLD hemodynamic response function was employed. For demonstrating the insular functional responses to the task localizers, we pooled the single subject GLM results together in a fixed-effects group analysis ($n = 2$) and overlaid results on the anatomical template's flat map (using Caret). To examine to what extent insular regions responded during the different tasks, we set significance level at $p < 0.001$, uncorrected.

3. Results

3.1. Functional responses in macaque insula

Figure 1 shows an overview of the functional responses in the insula (dashed white outline, regions outside the insula have been slightly masked out using a semi-transparent overlay) for the five different task localizers (see Suppl. Fig. 2 for the same figure without the semi-transparent mask). Contrasting sour and sweet liquid tastants versus distilled water yielded bilateral fMRI responses in the rostral portion of the insula, extending towards the most anterior end of the insula (Fig. 1A,F). Contrasting high vs low concentration of sour liquid tastants yielded differential responses also in the anterior portion of the insula (Fig. 1B,G), with a bias to the left hemisphere (Fig. 1B). Sensorimotor responses related to grasping objects with the right hand (compared to reaching-only) yielded bilateral differential responses in the middle of the insula (Fig. 1C,H), located posterior to the taste-sensitive region. These responses were stronger in the contralateral (Fig. 1C) hemisphere and encompassed both dorsal and ventral regions of the insula. At higher threshold ($p < 0.05$, corr.), grasping-related sensorimotor responses were prominent in particular in the dorsal portion of the middle insula. Bilateral galvanic vestibular stimulation yielded fMRI

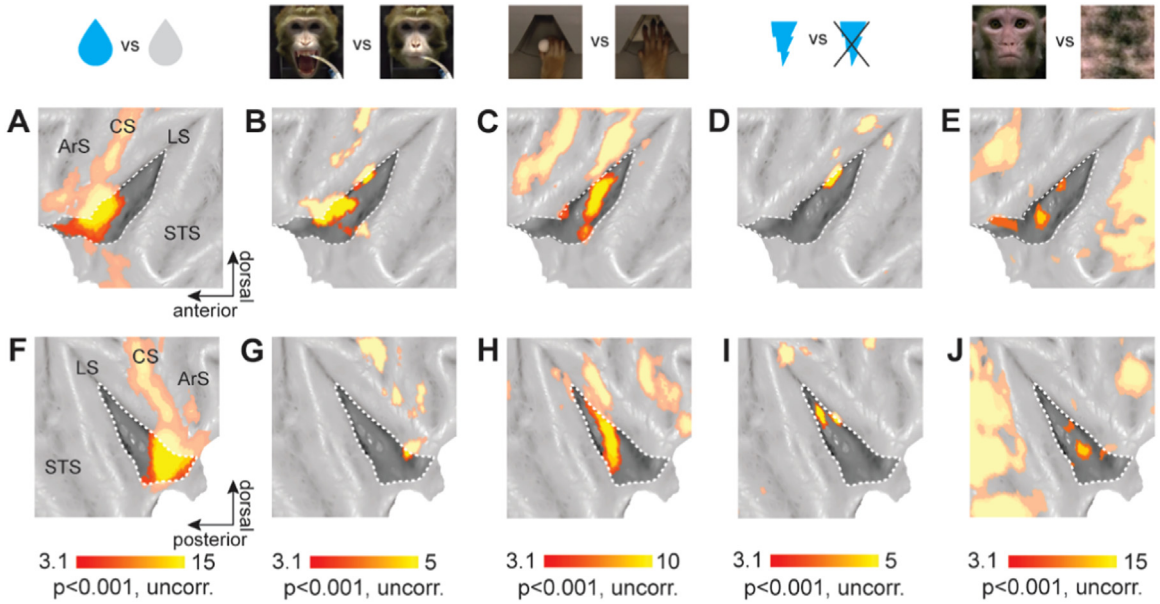

Fig. 1. Functional responses in the macaque insula. Univariate task-related fMRI responses (fixed-effects group results; n = 2) in left (**A – E**) and right insula (**F – J**) for the different task localizers. Extent of the insula is indicated with dashed white line and regions outside the insula are slightly masked out with semi-transparent overlay. **A,F.** Sweet and sour tastants vs. distilled water. **B,G.** High vs. low concentrated sour tastant. **C,H.** Reach-and-grasp execution vs. reach-only execution. **D,I.** Galvanic vestibular stimulation vs. no stimulation. **E,J.** Observation of lip-smacking facial gestures vs. scrambled controls.

responses in the posterior portion of the insula (Fig. 1D,I), with a right hemisphere bias (Fig. 1I). Finally, visual responses related to observing conspecific lip-smacking face expressions (compared to scrambled controls) yielded differential fMRI activity in several spots in middle and anterior portions of both dorsal and ventral insula (Fig. 1E,J). Overall, these functional MRI experiments suggest in particular a posterior to anterior insula representation of respectively vestibular, sensory-motor hand/arm, sensorimotor face and taste/distaste information.

3.2. Seed-to-whole-brain functional connectivity of macaque insula

To further examine the functional organization of the macaque insula, we performed a detailed seed-to-brain functional connectivity analysis with seeds along the entire extent of the dorsal and ventral insula (Figs. 2 and 3). For this purpose, eleven seeds (labelled B to L in left and N to X in right hemisphere respectively) were defined along the anterior-posterior extent of both the dorsal (Fig. 2A,M) and the ventral (Fig. 3A,M) insula in both hemispheres. For the dorsal insula (Fig. 2), the most anterior seeds (Fig. 2B-D and 2N-P) showed functional correlations in particular with ventral portions of the frontal part of the brain, as well as with visual cortex and STS. Seeds located in the middle portion of the dorsal insula showed a clear distinct functional connectivity pattern, yielding more pronounced functional correlations with dorsal regions including premotor, motor, cingulate and anterior parietal cortices (Fig. 2H-J and Fig. 2T-V). Most posterior dorsal insular seeds (Fig. 2L; Fig. 2X) on the other hand showed more restricted functional connectivity, in particular with posterior STS and lateral sulcus. In the ventral insula (Fig. 3), most anterior seeds showed functional correlations in particular with neighbouring regions in the anterior insula, lateral sulcus and frontal operculum, as well as with visual cortex (Fig. 3B; Fig. 3N). Seeds in the middle portion of the ventral insula showed functional connectivity with early visual, lower bank STS and parietal cortices (Fig. 3G,H; Fig. 3S,T). Similar to what was observed in the dorsal insula, the most posterior portion of the ventral insula yielded restricted functional connectivity with posterior STS and lateral sulcus, in addition to several early visual regions (Fig. 3L; Fig. 3X). Suppl. Figs 3 and 4 show which of the regions in the seed-to-brain functional connectivity maps survived false discovery rate correction and at which significance level for dorsal (Suppl. Fig 3) and ventral (Suppl. Fig 4) insular seeds. Overall, our seed-to-brain resting-state fMRI findings are in agreement with our task-based fMRI findings, showing a posterior to anterior transition of dorsal insular functional connections with respectively vestibular/optic flow regions, hand/arm sensorimotor, face sensorimotor, frontal opercular and orbitofrontal regions.

3.3. Seed-to-seed functional connectivity of macaque insula with functional networks

Next, to corroborate our findings of functional responses in the insula related to the task localizers, we examined in more detail insular functional connectivity with the vestibular/optic flow, sensorimotor grasping, gustatory/ingestive and social/affiliative networks. For each of the seeds in the insula, we plotted functional correlations (z-scores) with respectively four key regions belonging to each of aforementioned functional networks (Fig. 4, see methods for details with respect to ROI definition). Anterior dorsal insular seeds (Fig. 4A,B, dark blue colors) showed overall strongest functional connectivity with gustatory/ingestive regions including PrCO, DO, GrFO and mouth representation of F4 (Fig. 4A,B), and also with premotor F5a. For more posterior seeds located in the middle of the dorsal insula, functional correlations with gustatory/ingestive regions gradually diminished, while functional connectivity with in particular parietal portions of the sensorimotor grasping network (AIP, PE, hand representation of S1) as well as with vestibular/optic flow regions (VPS, MSTd and area 23) became stronger (Fig. 4A,B, light blue colors). The most posterior seeds in dorsal insula (Fig. 4A,B, purple colors) showed overall strongest functional connectivity with vestibular/optic flow regions VPS and MSTd. Anterior seeds in ventral portion of the insula showed strongest functional correlations with PrCO, DO and GrFO (Fig. 4C,D, dark blue colors). Towards the middle of the ventral insula, functional connectivity with gustatory/ingestive regions diminished while correlations increased with regions in the social/affiliative (in particular IPa and TEm), sensorimotor (area PE and hand representation of S1) and vestibular/optic flow (VPS, MSTd, area 23) networks (Fig. 4C,D, light blue colors). Overall

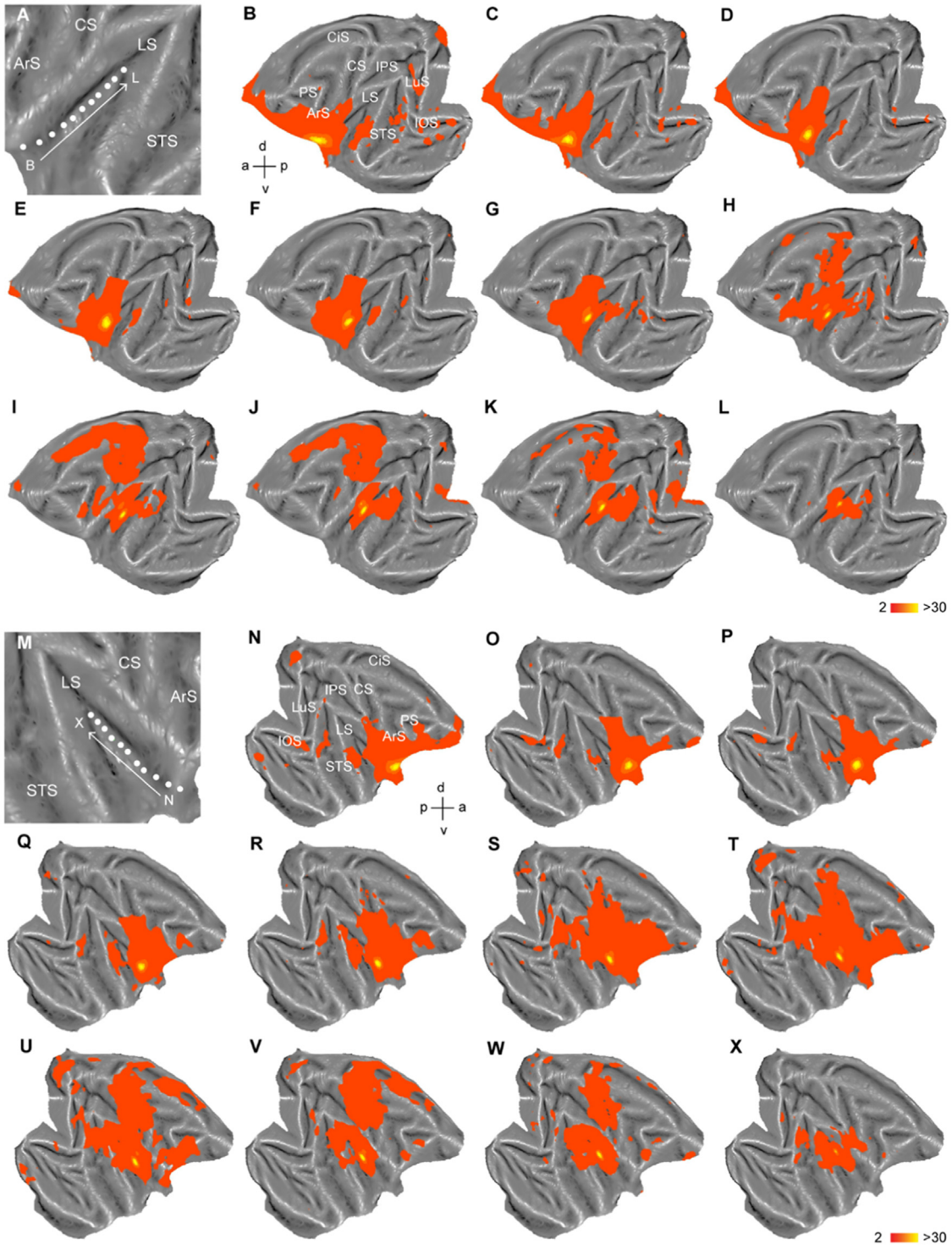

Fig. 2. Resting-state whole brain functional connectivity of the dorsal insula. A. Location of the seeds in dorsal portion of left insula. **B-L.** Ipsilateral seed-to-brain functional connectivity for distinct seeds across the anterior (B) to posterior (L) extent of the dorsal insula in left hemisphere. **M.** Location of the seeds in dorsal portion of right insula. **N-X.** Ipsilateral seed-to-brain functional connectivity for distinct seeds across the anterior (N) to posterior (X) extent of the dorsal insula in right hemisphere. All maps are thresholded at z > 2.0. IOS – inferior occipital sulcus; LuS – lunate sulcus; IPS – intraparietal sulcus; STS – superior temporal sulcus; LS – lateral sulcus; CS – central sulcus; CiS – cingulate sulcus; ArS – arcuate sulcus; PS – principal sulcus; a: anterior; p: posterior; d: dorsal; v: ventral.

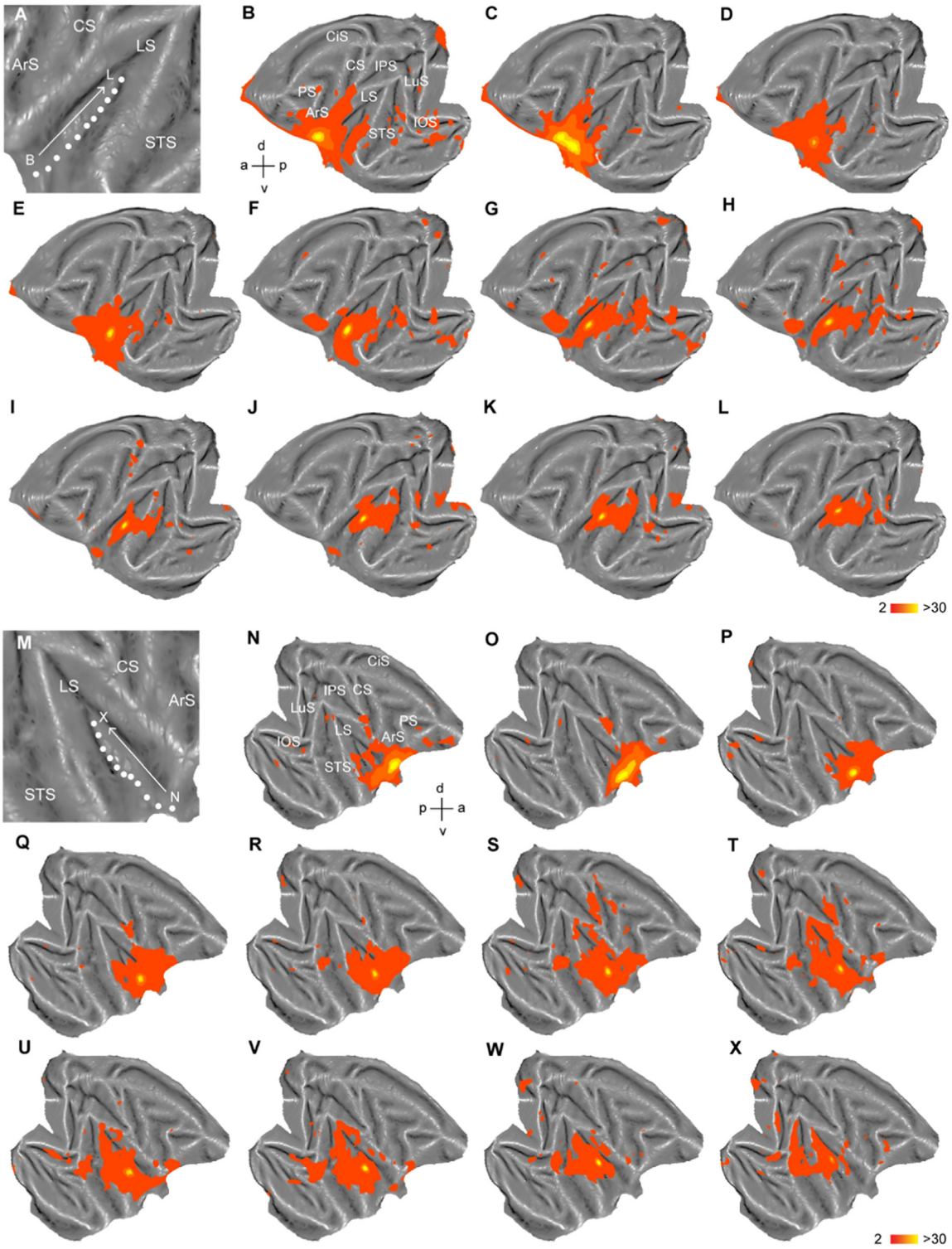

Fig. 3. Resting-state whole brain functional connectivity of the ventral insula. A. Location of the seeds in ventral portion of left insula. **B-L.** Ipsilateral seed-to-brain functional connectivity for distinct seeds across the anterior (B) to posterior (L) extent of the ventral insula in left hemisphere. **M.** Location of the seeds in ventral portion of right insula. **N-X.** Ipsilateral seed-to-brain functional connectivity for distinct seeds across the anterior (N) to posterior (X) extent of the ventral insula in right hemisphere. All maps are thresholded at $z > 2.0$. IOS – inferior occipital sulcus; LuS – lunate sulcus; IPS – intraparietal sulcus; STS – superior temporal sulcus; LS – lateral sulcus; CS – central sulcus; CiS – cingulate sulcus; ArS – arcuate sulcus; PS – principal sulcus; a: anterior; p: posterior; d: dorsal; v: ventral.

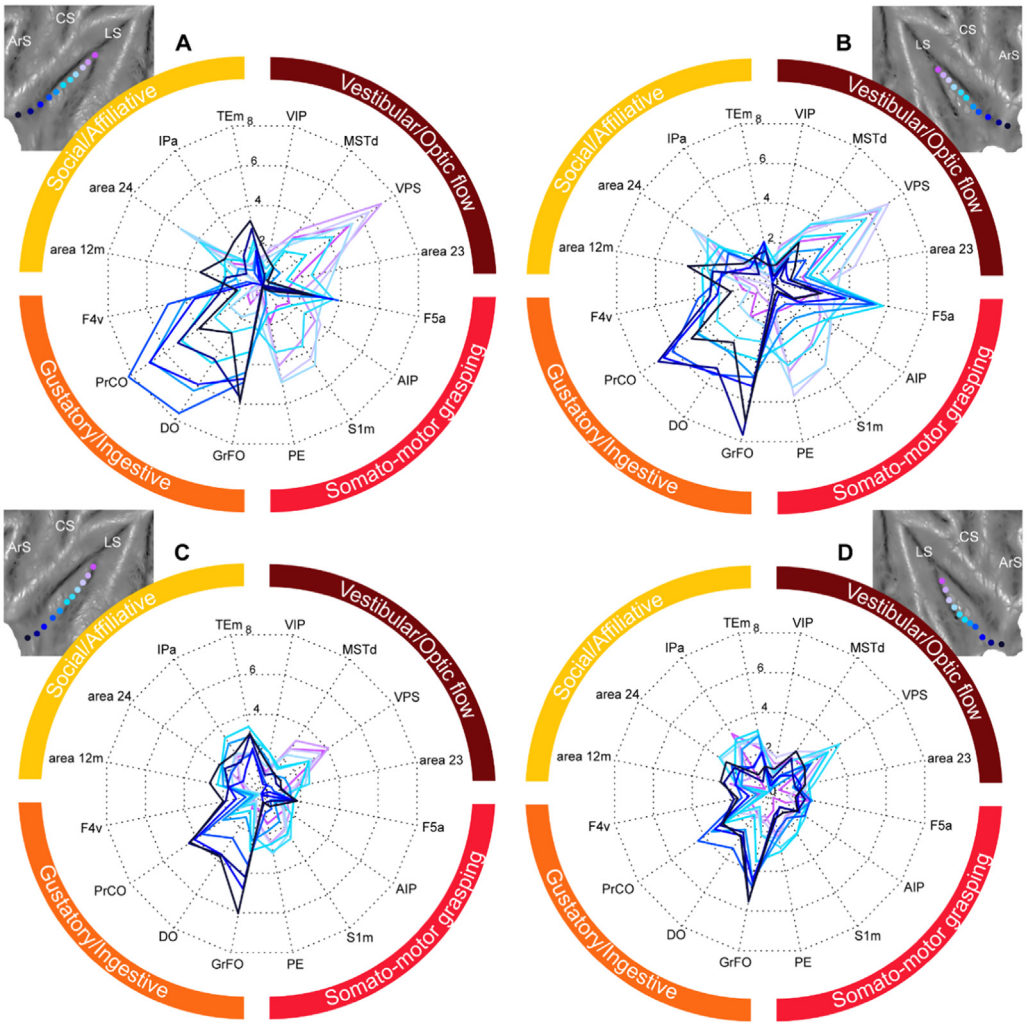

Fig. 4. Functional connectivity of insular seeds with vestibular, sensorimotor/grasping, gustatory/ingestive and social/affiliative brain networks. Spiderplots showing functional correlations (z-scores) of eleven seeds in respectively left and right dorsal (A,B) and left and right ventral (C,D) insula with key regions of the vestibular network, somatomotor or sensorimotor grasping network, gustatory/ingestive network and social/affiliative network. Colors of spiderplots correspond to the different seeds shown in the insets.

functional correlations of the posterior section of the ventral insula were weak, showing strongest functional connectivity with vestibular area VPS (Fig. 4C,D).

3.4. Functional connectivity gradients along antero-posterior extent of macaque insula

In order to summarize functional connectivity of the individual insular seeds with the four functional networks, we averaged all z-scores across each set of four ROIs belonging to the gustatory/ingestive, sensorimotor grasping, vestibular/optic flow and social/affiliative networks and plotted the average z-scores for each of the 44 insular seeds with these four networks (Fig. 5). Overall, the anterior portion of the dorsal insula showed strongest functional correlations with the gustatory/ingestive network (GrFO, DO, PrCO and F4v ROIs) with the most anterior seeds also showing functional connectivity with the social/affiliative network. Functional connectivity with the gustatory/ingestive/mouth motor regions diminished towards more posterior seeds located in the middle and posterior insula. The middle portion of the dorsal insula yielded significant functional correlations ($z > 2$) with the sensorimotor grasping and vestibular/optic flow networks. The most posterior portion of dorsal insula showed significant functional correlations ($z > 2$) with the vestibular/optic flow network (VIP, MSTd, VPS, area 23). Overall, for the dorsal insula (Fig. 5A,C), there was a clear trend of stronger functional connectivity with the gustatory/ingestive network for more anterior seeds and stronger functional connectivity with the sensorimotor grasping and vestibular/optic flow networks for more posterior seeds. While overall functional correlations of the dorsal insula with the social/affiliative network (area 12m, area 24, IPa, TEm) were generally weak, these correlations were strongest for the middle portion and the most anterior end of the dorsal insula.

For the ventral insula (Fig. 5B,D), the gustatory/ingestive network was functionally connected in particular with the anterior part (similar as for the dorsal insula), and this functional connectivity diminished towards more posterior seeds in the ventral insula. Comparing the middle portion of dorsal and ventral insula, a clear difference in functional connectivity strength with respective the social/affiliative and sensorimotor grasping networks was evident: while the middle ventral insula showed strongest functional correlations with the social/affiliative network seeds (area 12m, area 24, IPa, TEm) and less so with the sensorimotor grasping network (F5a, AIP, PE, hand representation of S1), this pattern was reversed for the dorsal portion of the middle insula (Fig. 5).

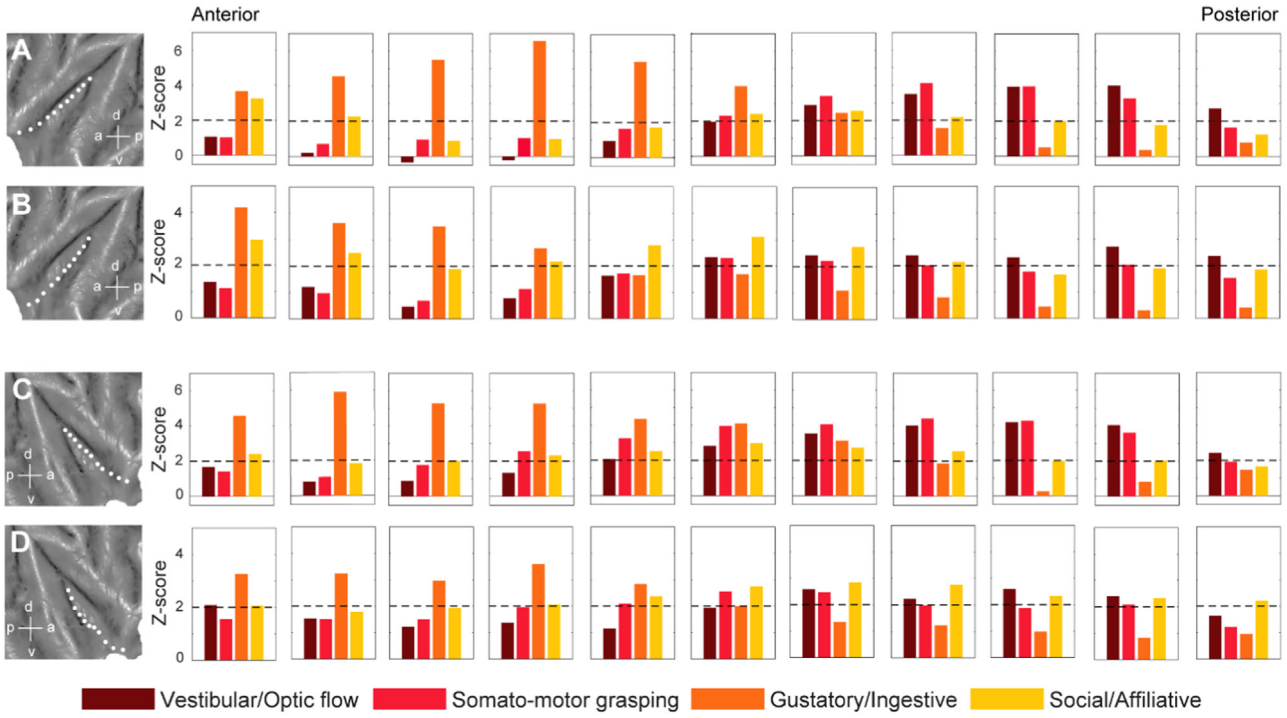

Fig. 5. Average functional connectivity of insular seeds with vestibular/optic flow, sensorimotor/grasping, gustatory/ingestive and social/affiliative brain networks. Average functional connectivity of eleven seeds in left dorsal (A), left ventral (B), right dorsal (C) and right ventral (D) insula with vestibular/optic flow network (bordeaux), sensorimotor grasping network (red), gustatory/ingestive network (orange) and social/affiliative network (yellow). a: anterior; p: posterior; d: dorsal; v: ventral.

4. Discussion

4.1. Vestibular responses in macaque insula

The exact role of the insula in processing vestibular information remains unclear. Processing of vestibular information in the Sylvian fissure of monkeys has been described in a functional region termed parieto-insular vestibular cortex (PIVC; Evrard, 2019) and in a more posterior region named visual posterior sylvian area (VPS; Chen et al., 2011). Functionally, PIVC differs from VPS in that the former is considered as a vestibular area while the latter is a visuo-vestibular area, integrating optic flow information in addition to the vestibular signals induced by self-motion. Although the exact spatial extent and location of PIVC is unclear, it overlaps mostly with the retroinsular cortex, adjacent to the posterior end of the insula but also includes part of the posterior insula (Grüsser et al, 1990; Akbarian et al., 1994; Chen et al., 2010, 2016). Our current results show that bilateral galvanic stimulation yields vestibular related responses in the posterior part of the insula (Fig. 1E,J), anterior to the retroinsular cortex, in line with a role in processing vestibular information. While responses were stronger in the right hemisphere, it is currently unclear if this finding reflects a real asymmetry in processing vestibular information in macaques, as has been reported in humans (Kirsch et al., 2018; Dieterich et al., 2003).

4.2. Grasping-related sensorimotor responses in macaque insula

In line with a previous monkey fMRI grasping study (Nelissen and Vanduffel, 2011), fMRI responses related to reaching-and-grasping in the dark (compared to reaching-only) yielded responses in the dorsal part of the middle insula, extending more anterior and ventral (Fig. 1C,H). This location, in particular the dorsal part of it, falls within the dorsal sensorimotor field of the insula. Previous single neuron studies suggest that this field is involved in somatosensory and motor processing (Robinson and Burton, 1980; Schneider et al., 1993; Jezzini et al., 2012; Ishida et al., 2015). The location of our hand movement related fMRI responses in the insula fits very well with a recent microstimulation study by Jezzini et al (2012). Electrical stimulation of the middle portion of the dorsal insula elicited mostly hand movements, while mouth and face movements could be elicited when stimulating different parts of the adjacent upper bank of the Sylvian fissure (Fig. 1A of Jezzini et al., 2012). Within the insula, ingestive movements involving the mouth were mostly observed after stimulating the region anterior to dorsal insula hand movement region (Fig. 1B of Jezzini et al., 2012), in a region corresponding to the one where we found taste/distaste/ingestive responses (see next paragraph). In line with a previous monkey fMRI grasping study (Nelissen and Vanduffel, 2011), our grasping localizer suggested that sensory-motor responses related to grasping extend antero-ventral into a region in the middle dysgranular insula (Fig. 1 C,H), referred to as a 'middle integration zone' (Evrard, 2022), possibly involved in integrating egocentric (own planned motor movements) and allocentric (context-dependent cues involving others) information. Both previous single cell and fMRI data showed that the portion of macaque insula where we observed grasping-related activity, does not only respond during execution of bodily actions but also during observation of others' actions (Ishida et al., 2015; Sharma et al., 2018), suggesting indeed that this region might play a role in integrating observed and experienced sensations and actions for guiding behaviour.

4.3. Gustatory/ingestive related responses in macaque insula

Single cell recordings indicate that the primary cortical taste region in monkeys is located in the anterior dorsal part of the insula (Scott et al., 1986; Yaxley et al., 1990), although the exact boundary and posterior/anterior or dorsal/ventral extent of this region is unclear. The location of our taste sensitive region in the anterior insula fits with the

results of another recent fMRI study that examined gustatory responses in the macaque (Kaskan et al., 2019). Although taste responses extended to the most anterior portion of the insula bordering the orbitofrontal cortex (Fig. 1A,F), the most anterior end of the insula might be functionally distinct from or more diverse than the slightly more posterior region where strongest responses for taste were observed (Evrard, 2022). Some evidence suggests the anterior end of the dorsal insula in macaques responds in particular during more complex cognitive tasks (Yang et al., 2022; Wang et al., 2015) and that in particular this anterior portion of the insula expanded significantly in the human brain compared to other primates (Bauernfeind et al., 2013; Evrard, 2019). Resting-state functional connectivity for this most anterior part of the insula indeed suggested distinct connectivity compared to neighbouring seeds located near the local maxima of the taste-responsive region (y = +19 mm), especially in terms of functional connectivity with visual cortices and ventrolateral prefrontal cortex (Fig. 2B,N). Microstimulation studies in monkeys suggest that the anterior insula is not only involved in processing of gustatory or ingestive information (chewing, swallowing, etc.), but that it also plays a role in the expression of emotional behaviour. Electrical stimulation of sites located in both the dorsal and ventral portions of the anterior insula elicited disgust-like behaviour in monkeys (Caruana et al., 2011; Jezzini et al., 2012). Our current taste and distaste/disgust data do not allow making any claims about the exact link between the observed fMRI responses and the sensory, emotional or motor aspects of the task, nor about possible different spatial representations for ingestive/taste processing versus distaste/disgust processing in the anterior insula. Both our taste and distaste/disgust localizer involved active ingestion of tastants and hence active mouth and licking movements in addition to oral somatosensory processing. Furthermore, as the high concentration sour condition in our distaste/disgust localizer also involved more facial movements related to distaste/disgust facial expressions compared to the low concentration sour condition, the differential fMRI responses that we observed could be related to taste intensity differences which also modulate neurons in the primary gustatory region of the anterior insula (Rolls, 2016), to the emotional aspects of distaste/disgust perception/experience and/or to the motor aspects of distaste/disgust facial expressions (Caruana et al., 2011; Jezzini et al., 2012). Future fMRI studies testing disgust responses to both gustatory as well as olfactory stimuli in monkeys might provide insights into the potential multimodal aspects of disgust processing in the anterior insula, as well as to what extent the taste/ingestive and disgust responses are represented in separate or overlapping subregions in the anterior insula. Interestingly, our data suggest stronger distaste/disgust responses in the left insula. While conclusive data is lacking at this point, some evidence points towards a left-lateralized processing of disgust also in humans (Holtmann et al., 2020, Calder et al., 2000, Papagno et al., 2016). A left-sided lateralization of disgust fits with the observation that left hemispheric stimulation of the anterior insula leads to parasympathetic activation (Oppenheimer et al., 1992; Caruana et al., 2011), the latter which has been linked to disgust (Stark et al., 2005).

4.4. Visual responses to conspecifics' lip-smacking facial gestures in macaque insula

Although functional evidence seems to indicate that the insula plays a crucial role in social communication, the exact contribution or involvement of different insular subsectors in processing stimuli depicting social information remains unclear. The middle portion of the ventral insula in macaques has been suggested to house a social (Evrard and Craig, 2015) or affiliative (Jezzini et al., 2015) field, while the more anterior portion would be part of an ingestive/disgust (Jezzini et al., 2015) or saliency network (Touroutoglou et al., 2016). Electrical stimulation of the middle to anterior portion of the ventral insula elicited affiliative lip-smacking motor behaviour, in particular during face-to-face interactions between the monkey and the experimenter (Caruana et al., 2011; Jezzini et al., 2012). In a recent monkey fMRI study, Shepherd and Freiwald (2018) described dorsal and anterior insular activity during production of lip-smacking gestures in monkeys, in line with the previously mentioned microstimulation studies (Caruana et al., 2011; Jezzini et al., 2012). Our current study shows that observation of lip-smacking gestures (compared to scrambled controls) causes activity in several spots in middle to anterior dorsal and ventral insula (Fig. 1E,J). These findings are in line with a previous monkey fMRI study that demonstrated face related responses in the anterior and ventral insula (Ku et al., 2011). Furthermore, together with the finding of single unit responses to conspecific vocalizations (Remedios et al., 2009), our results confirm the proposed role of the ventral insula in processing social cues conveying information from conspecifics (Jezzini et al., 2015; Evrard, 2019, 2022). Interestingly, strongest responses to observation of lip-smacking were observed in a portion of the middle/ventral dysgranular insula (Fig. 1 E,J), slightly anterior to the antero-ventral part of the grasping cluster (Fig. 1 C,H). While higher-resolution experiments (Li et al., 2022) would be needed to confirm this, this finding fits with the suggestion of a (rough) somatotopic representation in dysgranular insula proposed to receive input from adjacent somatotopically organized dorsal insular regions (Evrard, 2019, 2022). Recently developed two monkey fMRI setups (Cui and Nelissen, 2022; Gilbert et al., 2021) allow examining brain-wide processing of information related to own and others' behaviour (facial expressions and/or goal-directed hand motor acts) in more naturalistic social settings as compared to individual settings using virtual stimuli and might be highly relevant for examining the proposed role of the insula in integrating own and others' sensations and actions in social contexts for the purpose of guiding goal-directed or social behaviour.

4.5. Functional connectivity of macaque dorsal insula and comparison with tracer data

Besides employing a wide range of tasks to examine the functional responses of macaque insular subregions, we also examined to what extent resting-state fMRI could inform on the functional organization and role of different sectors of the insula. In line with tracer studies (Guldin et al., 1992; Mesulam and Mufson, 1982; Akbarian et al., 1994; Seltzer and Pandya, 1994; Evrard, 2019), seed-to-brain functional correlations of the posterior end of the insula showed functional connectivity mostly with adjacent retroinsular and visual posterior Sylvian (VPS) area, in addition to auditory and upper bank STS regions. Seed-to-ROI functional connectivity analysis of the posterior insula with several key regions processing vestibular and/or optic flow visual information consistent with self-motion (MSTd, VPS, VIP and posterior cingulate cortex) showed that the posterior insula functionally correlated most strongly with VPS, followed by MSTd and posterior cingulate area 23 (where pmCSv is located; De Castro et al., 2021), while correlations with VIP were generally weaker. These findings support the proposed role of the posterior insula as a multi-modal integration zone aiding self-motion perception (Cottereau et al., 2017; Chen et al., 2011; Evrard, 2019).

The middle portion of the dorsal insula showed functional correlations with several regions of the grasping motor network, including primary motor cortex, somatosensory cortices S1 and S2, premotor F5 and prefrontal area 46. Tracer studies as well as non-invasive diffusion measurements (di Cesare et al., 2019) suggest that this region is indeed connected to several regions of the grasping sensorimotor network (Borra et al., 2017). Seed-to-ROI functional connectivity analysis showed that this portion of the dorsal insula yielded strong functional correlations with the grasping network (areas AIP, PE and S1) as well as with vestibular regions VPS and cingulate cortex, fitting with its proposed role in integration somatosensory and interoceptive information for the purpose of planning and execution of goal-directed behaviour.

The anterior portion of the dorsal insula showed a clearly distinct functional connectivity profile compared to the more posterior part. In line with its role in integrating gustatory and somatosensory information (Rolls, 2016) aiding ingestive motor behaviour (Jezzini et al., 2012),

this region showed functional correlations with both regions processing gustatory information and mouth-movements in the frontal operculum and orbitofrontal cortex, in addition to the mouth representation within ventral portions of motor and premotor cortices. Our seed-to-ROI analysis showed that the anterior dorsal insula was functionally connected in particular to the frontal operculum regions GrFO, DO and PrCO, as well as to the mouth representation of F4 (F4v). Besides these regions, which presumably play a role in different sensory and motor aspects of feeding behaviour, premotor F5a also showed strong functional correlations with the anterior dorsal insula. While F5a is typically considered a hand motor region, tracer data suggest that this sector is not only connected with the middle portion of the dorsal insula where grasping motor responses are represented, but also with the anterior insula (Gerbella et al., 2011), pointing towards a possible role in integrating hand and mouth-related information subserving coordinated feeding behaviour.

4.6. Functional connectivity of macaque ventral insula and comparison with tracer data

Some functional and anatomical evidence suggests that the ventral insula plays a role in emotional and affective behaviour. Jezzini et al. (2015) refer to the middle portion of the ventral insula as an affiliative field, based upon specific affiliative social behaviours elicited when electrically stimulating this field (Caruana et al., 2011; Jezzini et al., 2012). In agreement with invasive tracer examinations (Jezzini et al., 2015), our results reveal that the middle portion of the ventral insula showed functional correlations in particular with several regions playing a role in processing social and affiliative information, including higher order visual regions in temporal cortex (TEm and IPa) which are involved in processing social cues of conspecifics (Perrett et al., 1989; Tsao and Livingstone, 2008), as well as orbitofrontal cortex (area 12) and anterior cingulate (area 24) involved in emotion processing and production of affiliative face gestures (Livneh et al., 2012; Jezzini et al., 2015).

As observed for the dorsal anterior insula, functional correlations of the ventral anterior insula were particularly strong with the frontal opercular regions GrFO, PrCO and DO belonging to the gustatory/ingestive network. In line with earlier tracer data (Jezzini et al., 2015), this anterior part of the ventral insula where ingestive and disgust related behaviour seems represented (Caruana et al., 2011; Jezzini et al., 2012), showed less functional connectivity to the higher order temporal areas (IPa and TEm). A direct comparison of functional correlations of dorsal and ventral insula with the four functional networks examined in this study (Fig. 5) suggest some clear differences. Significant functional connectivity with the social/affiliative network was particularly evident for the middle portion of the ventral insula, while the middle/posterior part of the dorsal insula showed overall stronger functional connectivity with the sensorimotor grasping and vestibular/optic flow networks. These observations agree well with a direct comparison of mid-dorsal and mid-ventral insular anatomical connectivity using invasive tracers (Jezzini et al., 2015).

Overall, our combined set of monkey fMRI experiments suggest both functional specialization and integration of vestibular, sensorimotor, gustatory and social information throughout distinct portions of the insula. While in this study we only examined static functional connectivity, approaches like dynamic functional connectivity, psychophysical interaction analysis (O'Reilly et al., 2012) or Granger causality analysis (Seth et al., 2015) might offer additional valuable insights into the dynamics of macaque insula's functional interactions between insular subregions and with other brain regions and networks. In particular, monkey fMRI studies combining precise focal reversible perturbations (Klink et al., 2021) with active tasks will be instrumental to reveal the exact causal contribution of macaque insular subregions to different aspects of cognition and behaviour (Evrard, 2019) and could provide valuable insights into behavioural and brain-wide network disturbances related to primate insular dysfunction.

Declaration of Competing Interest

none.

Credit authorship contribution statement

Lotte Sypré: Conceptualization, Methodology, Investigation, Formal analysis, Visualization, Writing – original draft, Writing – review & editing. **Jean-Baptiste Durand:** Methodology, Investigation, Formal analysis. **Koen Nelissen:** Conceptualization, Methodology, Investigation, Writing – original draft, Writing – review & editing, Supervision, Funding acquisition.

Data availability

Data will be made available on request.

Acknowledgements

The authors thank W. Depuydt, M. De Paep, C. Fransen, A. Hermans, P. Kayenbergh, D. Mantini, G. Meulemans, I. Puttemans, S. Sharma, C. Ulens and S. Verstraeten for technical and administrative support. This research was supported by Fonds Wetenschappelijk Onderzoek Vlaanderen (G.0.622.08; G.0.593.09; G.0.854.19) and KU Leuven (C14/17/109; C14/21/111).

Supplementary materials

Supplementary material associated with this article can be found, in the online version, at doi:10.1016/j.neuroimage.2023.120217.

References

Agcaoglu, O., Wilson, T.W., Wang, Y.P., Stephen, J., Calhoun, V.D., 2019. Resting state connectivity differences in eyes open versus eyes closed conditions. Human Brain Mapping 40 (8), 2488–2498. doi:10.1002/hbm.24539.

Akbarian, S., Grüsser, O.-J., Guldin, W.O., 1994. Corticofugal connections between the cerebral cortex and brainstem vestibular nuclei in the macaque monkeu. Journal of Comparative Neurology 339 (3), 421–437. doi:10.1002/cne.903390309.

Bauernfeind, A.L., de Sousa, A.A., Avasthi, T., Dobson, S.D., Raghanti, M.A., Lewandowski, A.H., et al., 2013. A volumetric comparison of the insular cortex and its subregions in primates. J. Hum. Evol. 64, 263–279. doi:10.1016/j.jhevol.2012.12.003.

Baumgärtner, U., Iannetti, G.D., Zambreanu, L., Stoeter, P., Treede, R.D., Tracey, I., 2010. Multiple somatotopic representations of heat and mechanical pain in the operculo-insular cortex: A high-resolution fMRI study. Journal of Neurophysiology 104 (5), 2863–2872. doi:10.1152/jn.00253.2010.

Baumgärtner, U., Tiede, W., Treede, R.D., Craig, A.D., 2006. Laser-evoked potentials are graded and somatotopically organized anteroposteriorly in the operculoinsular cortex of anesthetized monkeys. Journal of Neurophysiology 96 (5), 2802–2808. doi:10.1152/jn.00512.2006.

Belmalih, A., Borra, E., Contini, M., Gerbella, M., Rozzi, S., Luppino, G., 2009. Multimodal architectonic subdivision of the rostral part (area F5) of the macaque ventral premotor cortex. Journal of Comparative Neurology 512 (2), 183–217. doi:10.1002/cne.21892.

Benjamini, Y., Krieger, A.M., Yekutieli, D., 2006. Adaptive linear step-up procedures that control the false discovery rate. Biometrika 93, 491–507.

Borra, E., Gerbella, M., Rozzi, S., Luppino, G., 2017. The macaque lateral grasping network: A neural substrate for generating purposeful hand actions. Neurosci Biobehav Rev 75, 65–90. doi:10.1016/j.neubiorev.2017.01.017.

Calder, A. J., Keane, J., Manes, F., Antoun, N., & Young, A. W. (2000). Impaired recognition and experience of disgust following brain injury. Retrieved from http://neurosci.nature.com

Caruana, F., Jezzini, A., Sbriscia-Fioretti, B., Rizzolatti, G., Gallese, V., 2011. Emotional and social behaviors elicited by electrical stimulation of the insula in the macaque monkey. Current Biology doi:10.1016/j.cub.2010.12.042.

Chen, A., DeAngelis, G.C., Angelaki, D.E., 2011. Convergence of vestibular and visual self-motion signals in an area of the posterior sylvian fissure. Journal of Neuroscience 31 (32), 11617–11627. doi:10.1523/JNEUROSCI.1266-11.2011.

Chen, A., DeAngelis, G.C., Angelaki, D.E., 2010. Macaque parieto-insular vestibular cortex: Responses to self-motion and optic flow. Journal of Neuroscience 30 (8), 3022–3042. doi:10.1523/JNEUROSCI.4029-09.2010.

Chen, A., Gu, Y., Liu, S., DeAngelis, G.C., Angelaki, D.E., 2016. Evidence for a causal contribution of macaque vestibular, but not intraparietal, cortex to heading perception. Journal of Neuroscience 36 (13), 3789–3798. doi:10.1523/JNEUROSCI.2485-15.2016.

Chen, A., Zeng, F., DeAngelis, G.C., Angelaki, D.E., 2021. Dynamics of heading and choice-related signals in the parieto-insular vestibular cortex of macaque monkeys. Journal of Neuroscience 41 (14), 3254–3265. doi:10.1523/JNEUROSCI.2275-20.2021.

Cottereau, B.R., Smith, A.T., Rima, S., Fize, D., Héjja-Brichard, Y., Renaud, L., Lejards, C., Vayssière, N., Trotter, Y., Durand, J.B., 2017. Processing of Egomotion-Consistent Optic Flow in the Rhesus Macaque Cortex. Cereb Cortex 27 (1), 330–343. doi:10.1093/cercor/bhw412.

Cui, D., Nelissen, K., 2022. Two-monkey fMRI setup for investigating multifaceted aspects of social cognition and behavior involving a real-live conspecific. NeuroImage 255, 119187. doi:10.1016/j.neuroimage.2022.119187.

Cui, D., Sypré, L., Vissers, M., Sharma, S., Vogels, R., Nelissen, K., 2023. Categorization learning induced changes in action representations in the macaque STS. Neuroimage 265, 119780. doi:10.1016/j.neuroimage.2022.119780.

De Castro, V., Smith, A.T., Beer, A.L., Leguen, C., Vayssière, N., Héjja-Brichard, Y., Audurier, P., Cottereau, B.R., Durand, J.B., 2021. Connectivity of the Cingulate Sulcus Visual Area (CSv) in Macaque Monkeys. Cereb Cortex 31, 1347–1364. doi:10.1093/cercor/bhaa301.

Dieterich, M., Bense, S., Lutz, S., Drzezga, A., Stephan, T., Brandt, T., 2003. Dominance for vestibular cortical function in the non-dominant hemisphere. Cerebral Cortex; 13, 994–1007.

di Cesare, G., Pinardi, C., Carapelli, C., Caruana, F., Marchi, M., Gerbella, M., Rizzolatti, G., 2019. Insula connections with the parieto-frontal circuit for generating arm actions in humans and macaque monkeys. Cerebr Cortex 29, 2140–2147. doi:10.1093/cercor/bhy095.

Ekstrom, L.B., Roelfsema, P.R., Arsenault, J.T., Bonmassar, G., Vanduffel, W., 2008. Bottom-up dependent gating of frontal signals in early visual cortex. Science 321 (5887), 414–417. doi:10.1126/science.1153276.

Evrard, H.C., Craig, A.D., 2015. Insular cortex. In: Brain Mapping: An Encyclopedic Reference, 2, pp. 387–393. doi:10.1016/B978-0-12-397025-1.00237-2.

Evrard, H.C., 2019. The Organization of the Primate Insular Cortex. Frontiers in Neuroanatomy 13. doi:10.3389/fnana.2019.00043.

Evrard, H.C. (2022). Interoceptive integration in the primate insular cortex. Insular Epilepsies, 52-66. doi: 10.1017/9781108772396.007

Ferrari, P.F., Gerbella, M., Coudé, G., Rozzi, S., 2017. Two different mirror neuron networks: the sensorimotor (hand) and limbic (face) pathways. Neuroscience 358, 300–315. doi:10.1016/j.physbeh.2017.03.040.

Friston, K., Holmes, A., Worsley, K., Poline, J., Frith, C., Frackowiak, R., 1994. Statistical Parametric Maps in Functional Imaging: A General Linear Approach. Human Brain Mapping 2, 189–210.

Gerbella, M., Belmalih, A., Borra, E., Rozzi, S., Luppino, G., 2011. Cortical connections of the anterior (F5a) subdivision of the macaque ventral premotor area F5. Brain Structure and Function 216 (1), 43–65. doi:10.1007/s00429-010-0293-6.

Gerbella, M., Borra, E., Rozzi, S., Luppino, G., 2016. Connections of the macaque Granular Frontal Opercular (GrFO) area: a possible neural substrate for the contribution of limbic inputs for controlling hand and face/mouth actions. Brain Structure and Function 221 (1), 59–78. doi:10.1007/s00429-014-0892-8.

Gilbert, K.M., Cléry, J.C., Gati, J.S., Hori, Y., Johnston, K.D., Mashkovtsev, A., Selvanayagam, J., Zeman, P., Menon, R.S., Schaeffer, D.J., Everling, S., 2021. Simultaneous functional MRI of two awake marmosets. Nature Communications 12, 6608. doi:10.1038/s41467-021-26976-4.

Grüsser, O.J., Pause, M., Schreiter, U., 1990. Localization and responses of neurones in the parieto-insular vestibular cortex of awake monkeys (Macaca fascicularis). The Journal of Physiology 430 (1), 537–557. doi:10.1113/jphysiol.1990.sp018306.

Guldin, W.O., Akbarian, S., Grüsser, O.J., 1992. Cortico-cortical connections and cytoarchitectonics of the primate vestibular cortex: A study in the squirrel monkeys (Saimiri sciureus). Journal of Comparative Neurology 326 (3), 375–401. doi:10.1002/cne.903260306.

Holtmann, O., Bruchmann, M., Mönig, C., Schwindt, W., Melzer, N., Miltner, W.H.R., Straube, T., 2020. Lateralized deficits of disgust processing after insula-basal ganglia damage. Frontiers in Psychology 11 (1429). doi:10.3389/fpsyg.2020.01429.

Ishida, H., Suzuki, K., Grandi, L.C., 2015. Predictive coding accounts of shared representations in parieto-insular networks. Neuropsychologia 70, 442–454. doi:10.1016/j.neuropsychologia.2014.10.020.

Jezzini, A., Caruana, F., Stoianov, I., Gallese, V., Rizzolatti, G., 2012. Functional organization of the insula and inner perisylvian regions. Proceedings of the National Academy of Sciences of the United States of America 109 (25), 10077–10082. doi:10.1073/pnas.1200143109.

Jezzini, A., Rozzi, S., Borra, E., Gallese, V., Caruana, F., Gerbella, M., 2015. A shared neural network for emotional expression and perception: An anatomical study in the macaque monkey. Frontiers in Behavioral Neuroscience 9 (September). doi:10.3389/fnbeh.2015.00243.

Joly, O., Pallier, C., Ramus, F., Pressnitzer, D., Vanduffel, W., Orban, G.A., 2012. Processing of vocalizations in humans and monkeys: A comparative fMRI study. Neuroimage 62 (3), 1376–1389. doi:10.1016/j.neuroimage.2012.05.070.

Kaskan, P.M., Dean, A.M., Nicholas, M.A., Mitz, A.R., Murray, E.A., 2019. Gustatory responses in macaque monkeys revealed with fMRI: Comments on taste, taste preference, and internal state. NeuroImage 184, 932–942.

Kirsch, V., Boegle, R., Keeser, D., Kierig, E., Ertl-Wagner, B., Brandt, T., Dieterich, M., 2018. Handedness-dependent functional organizational patterns within the bilateral vestibular cortical network revealed by fMRI connectivity based parcellation. Neuroimage 178, 224–237.

Klink, P.C., Aubry, J.F., Ferrera, V.P., Fox, A.S., Froudist-Walsh, S., Jarraya, B., Konofagou, E.E., Krauzlis, R.J., Messinger, A., Mitchell, A.S., Ortiz-Rios, M., Oya, H., Roberts, A.C., Roe, A.W., Rushworth, M.F.S., Sallet, J., Schmid, M.C., Schroeder, C.E., Tasserie, J., Tsao, D.Y., Uhrig, L., Vanduffel, W., Wilke, M., Kagan, I., Petkov, C.I., 2021. Combining brain perturbation and neuroimaging in non-human primates. Neuroimage 235, 118017.

Kolster, H., Mandeville, J.B., Arsenault, J.T., Ekstrom, L.B., Wald, L.L., Vanduffel, W., 2009. Visual field map clusters in macaque extrastriate visual cortex. Journal of Neuroscience 29 (21), 7031–7039. doi:10.1523/JNEUROSCI.0518-09.2009.

Ku, S.-P., Tolias, A.S., Logothetis, N.K., Goense, J., 2011. FMRI of the face-processing network in the ventral temporal lobe of awake and anesthetized macaques. Neuron 70 (2), 352–362. doi:10.1016/j.neuron.2011.02.048.

Kurata, K., 2018. Hierarchical Organization Within the Ventral Premotor Cortex of the Macaque Monkey. Neuroscience 382, 127–143. doi:10.1016/j.neuroscience.2018.04.033.

Li, X., Zhu, Q., Vanduffel, W., 2022. Submillimeter fMRI reveals an extensive, fine-grained and functionally-relevant scene-processing network in monkeys. Prog Neurobiol 211, 102230. doi:10.1016/j.pneurobio.2022.102230.

Livneh, U., Resnik, J., Shohat, Y., Paz, R, 2012. Self-monitoring of social facial expressions in the primate amygdala and cingulate cortex. Proc. Natl. Acad. Sci. U S A 109, 18956–18961. doi:10.1073/pnas.1207662109.

Mantini, D., Corbetta, M., Romani, G.L., Orban, G.A., Vanduffel, W., 2012. Data-driven analysis of analogous brain networks in monkeys and humans during natural vision. Neuroimage 63, 1107–1118. doi:10.1016/j.neuroimage.2012.08.042.

Mantini, D., Gerits, A., Nelissen, K., Durand, J.-B., Joly, O., Simone, L., Vanduffel, W., 2011. Default Mode of Brain Function in Monkeys. Journal of Neuroscience 31 (36), 12954–12962. doi:10.1523/JNEUROSCI.2318-11.2011.

Maranesi, M., Rodà, F., Bonini, L., Rozzi, S., Ferrari, P.F., Fogassi, L., Coudé, G., 2012. Anatomo-functional organization of the ventral primary motor and premotor cortex in the macaque monkey. European Journal of Neuroscience 36 (10), 3376–3387. doi:10.1111/j.1460-9568.2012.08252.x.

Mesulam, M., Mufson, E.J., 1982. Insula of the Old World Monkey. I: Architectonics in the Insulo-orbito-temporal Component of the Paralimbic Brain. In THE JOURNAL OF COMPARATIVE NEUROLOGY 2.

Nelissen, K., Fiave, P.A., Vanduffel, W., 2018. Decoding Grasping Movements from the Parieto-Frontal Reaching Circuit in the Nonhuman Primate. Cerebral Cortex doi:10.1093/cercor/bhx037.

Nelissen, K., Luppino, G., Vanduffel, W., Rizzolatti, G., Orban, G.A., 2005. Observing others: Multiple action representation in the frontal lobe. Science 310 (5746), 329–332. doi:10.1126/science.1115740.

Nelissen, K., Vanduffel, W., 2011. Grasping-related functional magnetic resonance imaging brain responses in the macaque monkey. Journal of Neuroscience 31 (22), 8220–8229. doi:10.1523/JNEUROSCI.0623-11.2011.

Nelissen, K., Vanduffel, W., Orban, G.A., 2006. Charting the lower superior temporal region, a new motion-sensitive region in monkey superior temporal sulcus. Journal of Neuroscience 26 (22), 5929–5947. doi:10.1523/JNEUROSCI.0824-06.2006.

Ogawa, H., 1994. Gustatory cortex of primates: anatomy and physiology. Neuroscience Research 20 (1), 1–13. doi:10.1016/0168-0102(94)90017-5.

Oppenheimer, S.M., Gelb, A., Girvin, J.P., Hachinski, V.C., 1992. Cardiovascular effects of human insular cortex stimulation. Neurology 42, 1727–1732.

O'Reilly, J.X., Woolrich, M.W., Behrens, T.E., Smith, S.M., Johansen-Berg, H., 2012. Tools of the trade: psychophysiological interactions and functional connectivity. Soc Cogn Affect Neurosci 7, 604–609. doi:10.1093/scan/nss055.

Papagno, C., Pisoni, A., Mattavelli, G., Casarotti, A., Comi, A., Fumagalli, F., … Bello, L., 2016. Specific disgust processing in the left insula: New evidence from direct electrical stimulation. Neuropsychologia 84, 29–35. doi:10.1016/j.neuropsychologia.2016.01.036.

Parr, L.A., Waller, B.M., Burrows, A.M., Gothard, K.M., Vick, S.J., 2010. MaqFACS: A muscle-based facial movement coding system for the rhesus macaque. American Journal of Physical Anthropology 143 (4), 625–630. doi:10.1002/ajpa.21401.

Patel, G.H., Yang, D., Jamerson, E.C., Snyder, L.H., Corbetta, M., Ferrera, VP., 2015. Functional evolution of new and expanded attention networks in humans. Proc Natl Acad Sci U S A 112, 9454–9459. doi:10.1073/pnas.1420395112.

Patriat, R., Molloy, E.K., Meier, T.B., Kirk, G.R., Nair, V.A., Meyerand, M.E., … Birn, R.M., 2013. The effect of resting condition on resting-state fMRI reliability and consistency: A comparison between resting with eyes open, closed, and fixated. NeuroImage 78, 463–473. doi:10.1016/j.neuroimage.2013.04.013.

Peeters, R., Simone, L., Nelissen, K., Fabbri-Destro, M., Vanduffel, W., Rizzolatti, G., Orban, G.A., 2009. The representation of tool use in humans and monkeys: common and uniquely human features. J Neurosci 29, 11523–11539. doi:10.1523/JNEUROSCI.2040-09.2009.

Perrett, D.I., Harries, M.H., Bevan, R., Thomas, S., Benson, P.J., Mistlin, A.J., Chitty, A.J., Hietanen, J.K., Ortega, J.E., 1989. Frameworks of analysis for the neural representation of animate objects and actions. Journal of Experimental Biology 146, 87–113. doi:10.1242/jeb.146.1.87.

Pinsk, M.A., Arcaro, M., Weiner, K.S., Kalkus, J.F., Inati, S.J., Gross, C.G., Kastner, S., 2009. Neural representations of faces and body parts in macaque and human cortex: a comparative FMRI study. J Neurophysiol 101, 2581–2600. doi:10.1152/jn.91198.2008.

Remedios, R., Logothetis, N.K., Kayser, C., 2009. An auditory region in the primate insular cortex responding preferentially to vocal communication sounds. Journal of Neuroscience 29 (4), 1034–1045. doi:10.1523/JNEUROSCI.4089-08.2009.

Robinson, C.J., Burton, H., 1980. Somatic submodality distribution within the second somatosensory (SII), 7b, retroinsular, postauditory, and granular insular cortical areas of M. fascicularis. Journal of Comparative Neurology 192 (1), 93–108. doi:10.1002/cne.901920106.

Rolls, E.T., 2016. Functions of the anterior insula in taste, autonomic, and related functions. Brain and Cognition doi:10.1016/j.bandc.2015.07.002.

Schneider, R.J., Friedman, D.P., Mishkin, M., 1993. A modality-specific somatosensory area within the insula of the rhesus monkey. Brain Research 621 (1), 116–120. doi:10.1016/0006-8993(93)90305-7.

Scott, T.R., Yaxley, S., Sienkiewicz, Z.J., Rolls, E.T., 1986. Gustatory responses in the frontal opercular cortex of the alert cynomolgus monkey. Journal of Physiology 56 (3), 876–890. doi:10.1152/jn.1986.56.3.876.

Seltzer, B., Pandya, D.N., 1994. Parietal, temporal, and occipital projections to cortex of the superior temporal sulcus in the rhesus monkey: a retrograde tracer study. Journal of Comparative Neurology 343 (3), 445–463. doi:10.1002/cne.903430308.

Seth, A.K., Barrett, A.B., Barnett, L., 2015. Granger Causality Analysis in Neuroscience and Neuroimaging. J Neurosci 35 (8), 3293–3297. doi:10.1523/JNEUROSCI.4399-14.2015.

Sharma, S., Mantini, D., Vanduffel, W., Nelissen, K., 2019. Functional specialization of macaque premotor F5 subfields with respect to hand and mouth movements: A comparison of task and resting-state fMRI. NeuroImage doi:10.1016/j.neuroimage.2019.02.045.

Sharma, S., Fiave, P.A., Nelissen, K., 2018. Functional MRI Responses to Passive, Active, and Observed Touch in Somatosensory and Insular Cortices of the Macaque Monkey. The Journal of Neuroscience doi:10.1523/JNEUROSCI.1587-17.2018.

Sharma, S., Schaeffer, D.J., Vinken, K., Everling, S., Nelissen, K., 2021. Intrinsic functional clustering of ventral premotor F5 in the macaque brain. NeuroImage 227. doi:10.1016/j.neuroimage.2020.117647.

Shepherd, S.V., Freiwald, W.A., 2018. Functional networks for social communication in the Macaque monkey. Neuron 99 (2), 413–420. doi:10.1016/j.neuron.2018.06.027.

Spadone, S., Della Penna, S., Sestieri, C., Betti, V., Tosoni, A., Perrucci, M.G., Romani, G.L., Corbetta, M., 2015. Dynamic reorganization of human resting-state networks during visuospatial attention. Proc Natl Acad Sci U S A 112, 8112–8117. doi:10.1073/pnas.1415439112.

Stark, R., Walter, B., Schienle, A., Vaitl, D., 2005. Psychophysiological Correlates of Disgust and Disgust Sensitivity. J. Psychophysiol. 19 (1), 50–60.

Tagliazucchi, E., Laufs, H., 2014. Decoding wakefulness levels from typical fMRI resting-state data reveals reliable drifts between wakefulness and sleep. Neuron 82, 695–708. doi:10.1016/j.neuron.2014.03.020.

Touroutoglou, A., Bliss-Moreau, E., Zhang, J., Mantini, D., Vanduffel, W., Dickerson, B.C., Barrett, L.F., 2016. A ventral salience network in the macaque brain. NeuroImage 132, 190–197. doi:10.1016/j.neuroimage.2016.02.029.

Tsao, D., Livingstone, M., 2008. Mechanisms of face perception. Annual Review of Neuroscience 31, 411–437. doi:10.1146/annurev.neuro.30.051606.094238.

Vanduffel, W., Fize, D., Mandeville, J.B., Nelissen, K., Van Hecke, P., Rosen, B.R., … Orban, G.A., 2001. Visual motion processing investigated using contrast agent-enhanced fMRI in awake behaving monkeys. Neuron 32 (4), 565–577. doi:10.1016/S0896-6273(01)00502-5.

Vanduffel, W., Zhu, Q., Orban, G.A., 2014. Monkey cortex through fMRI glasses. Neuron 83, 533–550. doi:10.1016/j.neuron.2014.07.015.

Vincent, J.L., Patel, G.H., Fox, M.D., Snyder, A.Z., Baker, J.T., Van Essen, D.C., … Raichle, M.E., 2007. Intrinsic functional architecture in the anaesthetized monkey brain. Nature 447 (7140), 83–86. doi:10.1038/nature05758.

Wang, L., Uhrig, L., Jarraya, B., Dehaene, S., 2015. Representation of numerical and sequential patterns in macaque and human brains. Curr. Biol. 25, 1966–1974. doi:10.1016/j.cub.2015.06.035.

Yang, Y.P., Li, X., Stuphorn, V., 2022. Primate anterior insular cortex represents economic decision variables proposed by prospect theory. Nat Commun 13, 717. doi:10.1038/s41467-022-28278-9.

Yaxley, S., Rolls, E. T., & Sienkiewicz, Z. J. (1990). Gustatory Responses of Single Neurons in the Insula of the Macaque Monkey (Vol. 63).

Zhao, F., Wang, P., Hendrich, K., Ugurbil, K., Kim, S.G., 2006. Cortical layer-dependent BOLD and CBV responses measured by spin-echo and gradient-echo fMRI: Insights into hemodynamic regulation. NeuroImage 30 (4), 1149–1160. doi:10.1016/j.neuroimage.2005.11.013.